Observation of light-by-light scattering and new results from ultra-peripheral heavy-ion collisions in the ATLAS experiment

Y. Tayalati[*], **on behalf of the ATLAS collaboration**
Mohammed V University in Rabat
E-mail: tayalati@cern.ch

Light-by-light (LbyL) scattering, $\gamma\gamma \rightarrow \gamma\gamma$, is a very rare process allowed in Quantum Electrodynamics via a loop diagram. The precise measurement of this process is potentially sensitive to contributions from Beyond the Standard Model. Despite the small cross-section, the LbyL scattering can be observed in ultra-peripheral high energy heavy-ion collisions due to strong electromagnetic fields accompanying the lead beam. In this talk we discuss the first direct observation of LbyL scattering established by the ATLAS Collaboration using 2018 Pb+Pb dataset. We also summarize other new measurements done using ultra-peripheral events such as the measurement of multi-particle correlations and measurement of di-muon production.

The European Physical Society Conference on High Energy Physics -EPS-HEP-
10 - 17 July, 2019
Ghent, Belgium.

[*]Speaker.

PoS(EPS-HEP2019)317

1. Introduction

When ultra-relativistic beams of lead nuclei are brought into collision at the Large Hadron Collider (LHC), the most common processes studied are those for which the nuclei have an impact parameter less than twice their radius (b < 2R). At small or moderate b, such collisions are understood to create quark-gluon plasma and result in a large number of particles in the final state. However, the strong electromagnetic (EM) fields of the fully ionized nuclei can induce interactions even when the nuclei have significantly larger impact parameters such that no hadronic interaction occurs (b > 2R). In the equivalent photon approximation [1, 2], these strong EM fields correspond to a flux of quasi-real, high-energy photons. These photons can be emitted coherently from the entire nucleus, which enhances their flux by a factor of Z^2 (Z = 82 for Pb). These ultra-peripheral collisions (UPC) [3] have appreciable rates and include photon-photon and photo-nuclear interactions.

2. Standard Model light-by-light scattering

Light-by-light (LbyL) scattering, $\gamma\gamma \to \gamma\gamma$, process that is well predicted in quantum electrodynamics but forbidden in the classical theory of electrodynamics [4]. In the Standard Model (SM), the light-by-light scattering takes place at lowest order in the fine structure constant ($\alpha_{\rm em}$) via virtual one-loop box diagrams involving charged fermions (leptons and quarks) and the $W^{\pm}$ boson. The box diagrams shown in Figure 1 can also have extra contribution from beyond standard model particles likes axion-like particles.

The LbyL scattering is characterized by a very low cross section which makes its measurement very inaccessible but it can be observed in ultra-peripheral high energy heavy-ion collisions due to strong electromagnetic fields accompanying the lead beam . The first evidence of this process was measured using data taken during 2015 by both ATLAS [5] and CMS [6] . In this proceeding we present the observation of this process by the ATLAS experiment using the 2018 data.

The electromagnetic fields created by the colliding lead nuclei can be seen as a beam of quasi-real photons with a small virtuality of $Q^2 < 1/R^2$, where R is the radius of the charge distribution and so $Q^2 < 10^{-3}$ GeV^2[1, 2]. Then, the cross section for the reaction Pb+Pb $(\gamma\gamma) \to$ Pb+Pb $\gamma\gamma$ can be calculated by convolving the respective photon flux with the elementary cross section for the process $\gamma\gamma \to \gamma\gamma$. Since the photon flux associated with each nucleus scales as Z^2, the cross section is extremely increased with respect to proton–proton (pp) collisions.

3. Experimental evidences and new ATLAS measurements

3.1 The first ATLAS measurement

The first evidence of light-by-light scattering was reported by the ATLAS collaboration [5] after the analysis of data taken during 2015 lead-lead collisions at a center-of-mass energy per nucleon pair of 5.02 TeV by the ATLAS detector [7], the amount of data was 0.48 nb^{-1}. A total of 13 candidate events were observed with an expected background of 2.6± 0.7. Figure 2 shows the invariant mass of the diphoton system for the resulting events. Similar results were late published by the CMS collaboration [6] .

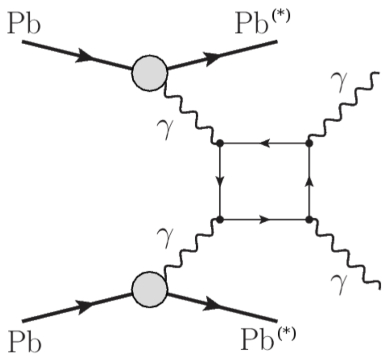

Figure 1: Schematic diagram of light-by-light scattering in UPC PbPb collisions. A potential electromagnetic excitation of the outgoing Pb ions is denotes by $(^*)$.

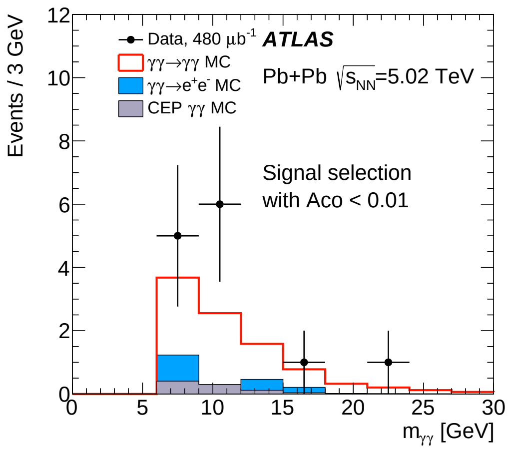

Figure 2: Invariant mass off the diphoton system after applying all the selections. Data (points) are compared with the sum of signal and background expectations (histograms) [5].

3.2 The new measurement

3.2.1 Event selection

The final-state signature of interest is the exclusive production of two photons, Pb+Pb $(\gamma\gamma) \rightarrow$ Pb$^{(*)}$+Pb$^{(*)}$ $\gamma\gamma$, where the diphoton final-state is measured in the central detector, and the incoming Pb ions survive the EM interaction, with a possible EM excitation [8], denoted by $(^*)$. Hence, the final state consists of two low-energy photons and no further activity in the detector, and in particular no reconstructed charged-particle tracks originating from the interaction point. The analysis follows the same approach of the initial ATLAS measurement, which was originally proposed in Ref. [9].

3.2.2 Backgrounds

The exclusive diphoton final state can also be produced via the strong interaction through a quark loop in the exchange of two gluons in a color-singlet state as shown in Figure 3(a). This central exclusive production (CEP) process, $gg \rightarrow \gamma\gamma$, was simulated using SuperChic v3.0. This

process has a large theoretical uncertainty, of $\mathcal{O}(100\%)$ [10], hence the absolute normalization of this background is determined using data driven method.
The $\gamma\gamma \to e^+e^-$ process as shown in Figure 3(b) is a potential background when both leptons are reconstructed as photons, but is also used for calibration studies in the analysis. The process was modeled with the Starlight 2.0 generator. Its production cross section is computed by combining the Pb+Pb photon flux with the leading-order formula for $\gamma\gamma \to e^+e^-$. Two-photon production of quark–antiquark pairs, with their subsequent decay into multiple hadrons, was modeled using HERWIG++ 2.7.1 [11], where the initial photon fluxes from pp collisions are implemented. The sample was then normalized to cover the differences in the photon fluxes between PbPb and pp collisions. All simulated events make use of a detector simulation [12] based on GEANT4 [13] and are reconstructed with the standard ATLAS reconstruction software.

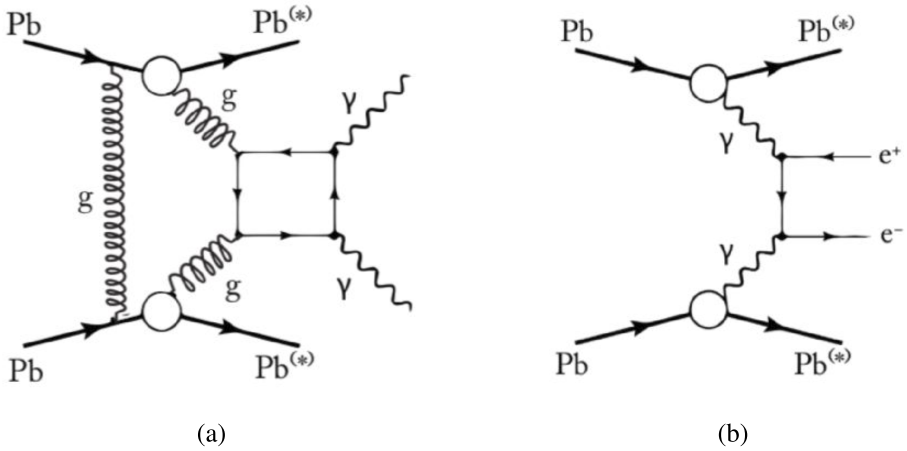

Figure 3: Feynman diagrams for central exclusive production $gg \to \gamma\gamma$ (a) and $\gamma\gamma \to e^+e^-$ process (b) in lead lead collisions .

3.2.3 Photon Performance studies

Photons reconstruction is done using EM clusters in the calorimeter [14] and tracking information from the Inner Detector, which allows to identify photon conversions [15]. An energy calibration specifically optimized for photons [16] is applied to account for energy loss before the calorimeter and both lateral and longitudinal shower leakage. Photons in MC samples are corrected [15] for known mismodeling of quantities that describe the properties ("shapes") of the associated EM showers. The photon reconstruction efficiency is extracted from data using $\gamma\gamma \to e^+e^-$ events, where one of the electrons emits a hard bremsstrahlung photon due to interaction with the material of the detector. The analysis is performed for events with exactly one identified electron and exactly two reconstructed charged-particle tracks, and a tag-and-probe method is used as described in Ref. [5]. The resulting photon reconstruction efficiency is shown in Figure 4(a). It rises from about 60% at E_T = 2.5 GeV to 90% at E_T = 6 GeV and is used to derive simulation-to-data correction factors. Based on these studies, MC events are corrected using photon E_T-dependent simulation-to-data correction factors. The systematic uncertainty on the photon reconstruction and particle identification (PID) efficiencies is estimated by parameterizing the correction factors as a function of the photon η instead of the photon E_T.

The photon PID in this analysis is based on a selection of these shower-shape variables, optimized for the signal events. Only photons with $E_T > 3$ GeV and $|\eta| < 2.37$, excluding the calorimeter transition region $1.37 < |\eta| < 1.52$, are considered. This allows for good separation between prompt photons and fake signatures due to calorimeter noise, cosmic-ray muons, or non-prompt photons originating from the decay of neutral hadrons. The photon PID is based on a neural network trained on background photons extracted from data and on photons from the signal MC sample. The selection of background photons follows the procedure established in Ref. [5].

High-p_T exclusive dilepton production ($\gamma\gamma \to \ell^+\ell^-$, where $\ell = e,\ \mu$) with final-state radiation (FSR) is used to measure the photon PID efficiency, defined as the probability for a reconstructed photon to satisfy the identification criteria. Events with exactly two oppositely charged tracks with $p_T > 0.5$ GeV are selected from UPC triggered events. In addition, a requirement to reconstruct a photon candidate with $E_T > 2.5$ GeV and $|\eta| < 1.37$ or $1.52 < |\eta| < 2.37$ is imposed. A photon candidate is required to be separated from each track by fulfilling $\Delta R > 0.3$ [17] to avoid leakage between the photon and the electron clusters. The FSR event candidates are required to have $p_T^{\ell\ell\gamma} < 1$ GeV requirement, where $p_T^{\ell\ell\gamma}$ is the transverse momentum of the three-body system consisting of the two tracks and the photon candidate. Figure 4(b) shows the photon PID efficiency as a function of reconstructed photon E_T, where the measurement from data is compared with the one extracted from the signal MC sample.

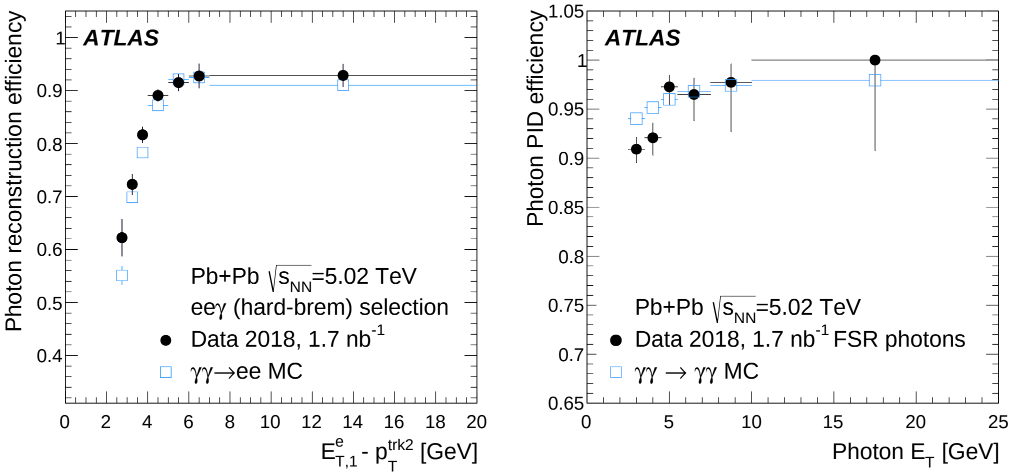

(a) (b)

Figure 4: (a) photon reconstruction efficiency as a function of the photon E_T (approximated with $E^e_{T,1} - p_T^{\text{trk2}}$, where trk2 denotes the track of the second leading electron), and (b) photon particle-identification efficiency as a function of the photon E_T [18].

The acoplanarity: $A_\phi = (1 - |\Delta\phi_{\gamma\gamma}|/\pi) < 0.01$ requirement significantly reduces the CEP $gg \to \gamma\gamma$ background. Its remaining contribution is evaluated from a control region defined by applying the same selection as for the signal region, but inverting the A_ϕ requirement to $A_\phi > 0.01$, and correcting the measured event yield for the expected signal and $\gamma\gamma \to e^+e^-$ contributions. The CEP and $\gamma\gamma \to e^+e^-$ processes exhibit a significantly broader A_ϕ distribution than the $\gamma\gamma \to \gamma\gamma$ process. Figure 5(a) shows the acoplanarity distrubtion before applyiong the $A_\phi < 0.01$ cut .

3.2.4 measurement results

After applying the signal selection, 59 events are observed in the data where 30 ± 4 (syst.) signal events and 12 ± 1 (stat.) ± 3 (syst.) background events are expected. Figure 5(b) shows the invariant mass for photons satisfying all selection criteria. The probability that the data is compatible with the background-only hypothesis was evaluated in a narrower $0 < A_\phi < 0.005$ range, which in studies using simulated data was found to be most sensitive. In this region, 42 events are observed in the data where 25 ± 3 (syst.) signal events and 6 ± 1 (stat.) ± 2 (syst.) background events are expected.

The measured fiducial cross section is 78 ± 13 (stat.) ± 7 (syst.) ± 3 (lumi.) nb, which can be compared with the predicted values of 45 ± 5 nb from Ref. [9], 51 ± 5 nb from Ref. [19] and 50 ± 5 nb from SuperChic3 MC simulation [20].

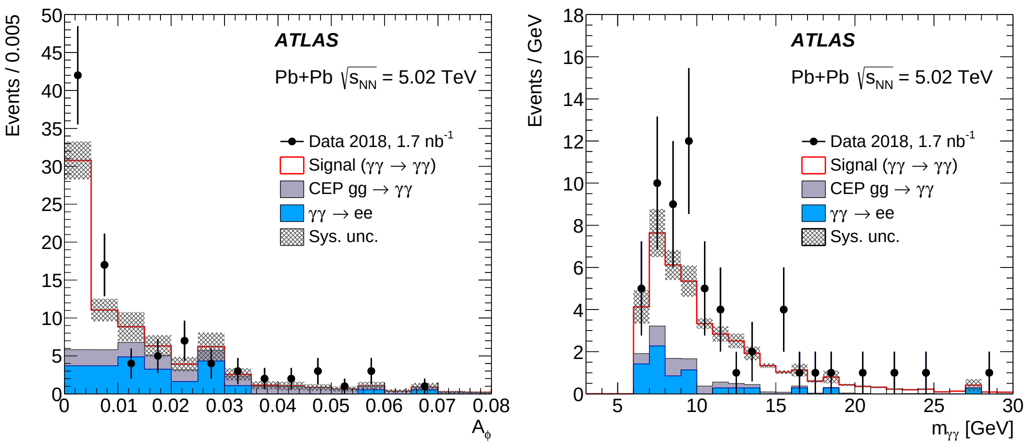

(a) (b)

Figure 5: (a) The diphoton A_ϕ distribution for events satisfying the signal selection, but before the $A_\phi < 0.01$ requirement. (b) Diphoton invariant mass for events satisfying the signal selection. Data (points) are compared with the sum of signal and background expectations (histograms). Systematic uncertainties of the signal and background processes, excluding that of the luminosity, are shown as shaded bands[18].

4. New results from ultra-peripheral heavy-ion collisions (UPC)

This section is dedicated to a summary of a measurement of two-particle long-range azimuthal correlations in photo-nuclear collisions using 1.73 $\text{nb}^{-1}$of 5.02 TeV Pb+Pb data collected in 2018 by ATLAS with a dedicated photo-nuclear event trigger [21]. Candidate photo-nuclear events are selected using a combination of the zero-degree calorimeters, forward calorimeters, and reconstructed pseudorapidity gaps constructed from calorimeter clusters and charged-particle tracks. Correlation functions as shown in Figure 6 are formed using charged-particle tracks in the event.

A template fitting method is employed to subtract the non-flow contribution. Second-order (elliptic) flow coefficients are presented as a function of charged-particle multiplicity and transverse momentum, and significant non-zero values of the flow coefficients are observed. The results are compared to flow coefficients obtained in proton–proton and proton–lead collisions in similar multiplicity ranges as shown in Figure 7.

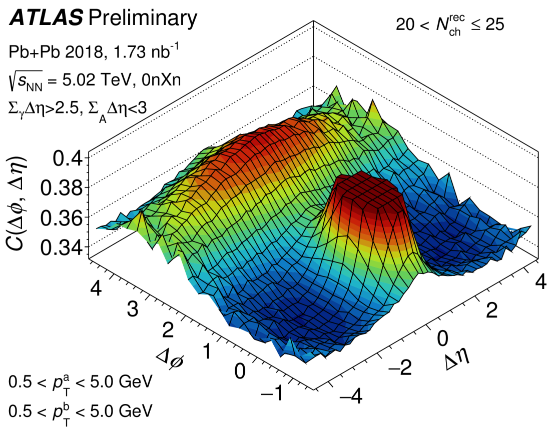

Figure 6: Two-dimensional normalized particle pair distributions in photo-nuclear events, corrected for acceptance effects with the mixed event distribution, and presented as a function of $\Delta\eta$ and $\Delta\phi$. The peak at $\Delta\phi = 0$ $\Delta\eta = 0$ is truncated to better show the structure of the correlation function.This panel corresponds to the range $20 < N_{\mathrm{ch}}^{\mathrm{rec}} < 25$ of charged-particle multiplicity [21].

5. Conclusion

This proceedings describe the observation of light-by-light scattering in ultraperipheral PbPb collisions at $\sqrt{s_{\mathrm{NN}}} = 5.02$ TeV recorded in 2018 by the ATLAS experiment in one hand and report a measurement of long-range two-particle correlations in high-energy photo-nuclear collisions using the same dataset in the other hand. Concerning light-by-light scattering 59 data events are observed in the signal region, while 12 ± 3 background events are expected. The photo nuclear analysis shows that the correlation function in high-multiplicity photo-nuclear events can be described as the sum of a contribution from low-multiplicity events and a pedestal with Fourier coefficient modulations. The single particle coefficients v2 are reported as a function of charged-particle multiplicity and single-particle p_{T}, and are compared to those previously measured in *pp* and *p*+Pb events. Ultraperipheral PbPb collisions will improve the understanding of the strong electromagnetic fields surrounding the nucleus, which enable future UPC measurements utilizing these high energy probes

PoS(EPS-HEP2019)317

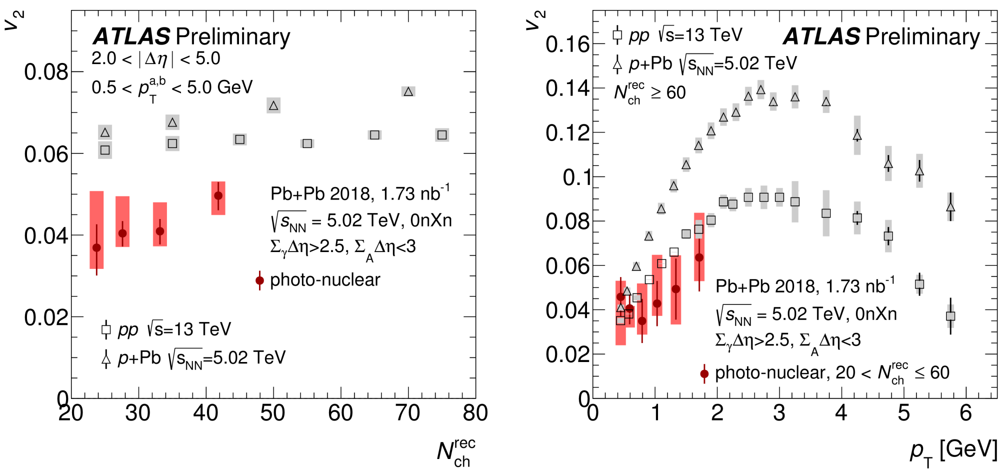

(a) (b)

Figure 7: (a) Flow coefficients v2 for charged particles with $0.5 < p_T < 5.0$ GeV in photo-nuclear events, as a function of charged-particle multiplicity N_{ch}^{rec}. (b) Charged-particle flow coefficients v2 in photo-nuclear events with $20 < N_{ch}^{rec} \leq 60$, as a function of particle p_T. The vertical error bars and colored boxes represent the statistic and total systematic uncertainties, respectively. The photo-nuclear data points are positioned at the average p_T value in each intervals. The data are compared to the analogous measurements in *pp* and *p*+Pb collisions [21].

References

[1] E. Fermi, *On the theory of collisions between atoms and electrically charged particles*, Nuovo Cim. **2** (1925) 143–158, arXiv:hep-th/0205086.

[2] E. J. Williams, *Nature of the High Energy Particles of Penetrating Radiation and Status of Ionization and Radiation Formulae*, Phys. Rev. **45** (1934) 729–730.

[3] C. A. Bertulani, S. R. Klein, and J. Nystrand, *PHYSICS OF ULTRA-PERIPHERAL NUCLEAR COLLISIONS*, Annual Review of Nuclear and Particle Science **55** no.~1, (2005) 271âĂŞ310, http://dx.doi.org/10.1146/annurev.nucl.55.090704.151526.

[4] W. Heisenberg and H. Euler, *Consequences of Dirac's theory of positrons*, Z. Phys. **98** no.~11, (1936) 714–732, arXiv:physics/0605038.

[5] ATLAS Collaboration, *Evidence for light-by-light scattering in heavy-ion collisions with the ATLAS detector at the LHC*, Nature Phys. **13** no.~9, (2017) 852–858, arXiv:1702.01625 [hep-ex].

[6] CMS Collaboration, *Evidence for light-by-light scattering and searches for axion-like particles in ultraperipheral PbPb collisions at $\sqrt{s_{NN}}$ = 5.02TeV*, Physics Letters B **797** (2019) 134826, http://dx.doi.org/10.1016/j.physletb.2019.134826.

[7] ATLAS Collaboration, *The ATLAS experiment at the CERN Large Hadron Collider*, JINST **3** (2008) S08003.

[8] ALICE Collaboration, *Measurement of the Cross Section for Electromagnetic Dissociation with Neutron Emission in Pb-Pb Collisions at $\sqrt{s_{NN}}$ = 2.76 TeV*, Phys. Rev. Lett. **109** (2012) 252302, arXiv:1203.2436 [nucl-ex].

[9] D. d'Enterria and G. G. da Silveira, *Observing Light-by-Light Scattering at the Large Hadron Collider*, Phys. Rev. Lett. **111** (2013) 080405, [Erratum: Phys. Rev. Lett. **116** (2016) 129901], arXiv:1305.7142 [hep-ph].

[10] CDF Collaboration, T. Aaltonen et al., *Observation of Exclusive $\gamma\gamma$ Production in $p\bar{p}$ Collisions at* $\sqrt{s} = 1.96$ *TeV*, Phys. Rev. Lett. **108** (2012) 081801, arXiv:1112.0858 [hep-ex].

[11] M. Bähr et al., *Herwig++ physics and manual*, Eur. Phys. J. C **58** (2008) 639–707, arXiv:0803.0883 [hep-ph].

[12] ATLAS Collaboration, *The ATLAS Simulation Infrastructure*, Eur. Phys. J. C **70** (2010) 823–874, arXiv:1005.4568 [physics.ins-det].

[13] GEANT4 Collaboration, *GEANT4 – a simulation toolkit*, Nucl. Instrum. Meth. A **506** (2003) 250–303.

[14] ATLAS Collaboration, *Electron and photon reconstruction and performance in ATLAS using a dynamical, topological cell clustering-based approach*, Tech. Rep. ATL-PHYS-PUB-2017-022, CERN, Geneva, Dec, 2017. https://cds.cern.ch/record/2298955.

[15] ATLAS Collaboration, *Measurement of the photon identification efficiencies with the ATLAS detector using LHC Run 2 data collected in 2015 and 2016*, Eur. Phys. J. C **79** (2019) 205, arXiv:1810.05087 [hep-ex].

[16] ATLAS Collaboration, *Electron and photon energy calibration with the ATLAS detector using 2015-2016 LHC proton-proton collision data*, JINST **14** (2019) P03017, arXiv:1812.03848 [hep-ex].

PoS(EPS-HEP2019)317

[17] ATLAS uses a right-handed coordinate system with its origin at the nominal interaction point (IP) in the center of the detector and the z-axis along the beam pipe. The x-axis points from the IP to the center of the LHC ring, and the y-axis points upward. Cylindrical coordinates (r,ϕ) are used in the transverse plane, ϕ being the azimuthal angle around the z-axis. The pseudorapidity is defined in terms of the polar angle θ as $\eta = -\ln\tan(\theta/2)$. The distance between two objects in η–ϕ space is $\Delta R = \sqrt{(\Delta\eta)^2 + (\Delta\phi)^2}$. Transverse momentum is defined by $p_T = p\sin\theta$.

[18] ATLAS Collaboration, *Observation of Light-by-Light Scattering in Ultraperipheral Pb+Pb Collisions with the ATLAS Detector*, Physical Review Letters **123** no.~5, (2019), http://dx.doi.org/10.1103/PhysRevLett.123.052001.

[19] M. Klusek-Gawenda, P. Lebiedowicz, and A. Szczurek, *Light-by-light scattering in ultraperipheral Pb-Pb collisions at energies available at the CERN Large Hadron Collider*, Phys. Rev. C **93** no.~4, (2016) 044907, arXiv:1601.07001 [nucl-th].

[20] L. A. Harland-Lang, V. A. Khoze, and M. G. Ryskin, *Exclusive LHC physics with heavy ions: SuperChic 3*, Eur. Phys. J. C **79** no.~1, (2019) 39, arXiv:1810.06567 [hep-ph].

[21] ATLAS Collaboration, *Two-particle azimuthal correlations in photo-nuclear ultra-peripheral Pb+Pb collisions at 5.02 TeV with ATLAS*, Tech. Rep. ATLAS-CONF-2019-022, CERN, Geneva, Jun, 2019. https://cds.cern.ch/record/2679473.

PoS(EPS-HEP2019)317